J Electr Eng Technol.2018; 13(5): 1908-1916
http://doi.org/10.5370/JEET.2018.13.5.1908

ISSN(Print) 1975-0102
ISSN(Online) 2093-7423

Design of Robust Resonance Suppression Controller in Parameter Variation for Speed Control of Parallel Connected Dual SPMSMs Fed by a Single Inverter

Chul Yun*, Tae-Sung Jang*, Nae-Soo Cho, Byung-Keun Yoon*** and Woo-Hyen Kwon†**

Abstract – This paper proposes a controller design method for suppressing the resonance generated in the slave motor in the middle and low speed operation range, according to the load and parameter differences between two motors, during parallel operation using the master and slave method that controls two surface permanent magnet synchronous motors connected in parallel by a single inverter. The proposed resonance suppression controller is directly obtained by analyzing the resonance characteristics, using the lead controller method. Therefore, it is possible to fundamentally reduce trial and error to set the controller gain. In addition, because the proposed resonance suppression controller was designed as a lead controller, the stability region of the system increased owing to the added zero point, making the system robust with respect to parametric variations. Simulations and experiments confirmed the usefulness of the proposed method and the system's robustness with respect to parametric variations.

Keywords: Dual SPMSMs, SIMM, Resonance characteristic analysis, Lead controller.

1. Introduction

Many surface permanent magnet synchronous motors (SPMSM) are driven as fan motors for heat exchange between air and refrigerants in outdoor air conditioning units in large buildings.

Even if multiple SPMSMs are used in the same system for a simple purpose, the same number of inverters is required for driving SPMSMs, which increases the manufacturing cost of the system. Therefore, there is a need to develop a single inverter multiple motor (SIMM) control technique, as schematically shown in Fig. 1. Several studies have been conducted to that end [1-6].

The master and slave control method, in which only the master motor is controlled, is one of the several SIMM methods that have been proposed. In this system, a heavy load motor is defined as a master (main) motor while a light load motor is defined as a slave (auxiliary) motor. However, when the load of the auxiliary motor becomes larger than that of the main motor, the control object must be changed. In presently available systems, a transient state occurs when the control variable is changed; as a consequence, the system may be damaged. Therefore, even if the load is changed, when the motor to be controlled is fixed, the auxiliary motor tends to synchronize with the input frequency owing to the resonance characteristics of the energy coupling between the two motors in the speed (middle and low) area, and the stator resistance cannot be ignored [7, 8]. In other words, the difference between the characteristics of the two motors appears as a difference between their torque angles, which induces a resonance in the auxiliary motor, which in turn contributes to the destabilization of the SIMM system. This resonance is a major hurdle that prevents commercialization of this system, because it reduces the reliability of the SIMM system.

To solve the problem of the resonance, active damping control methods have been considered [9-13]. Active damping increases the damping gain, and uses the

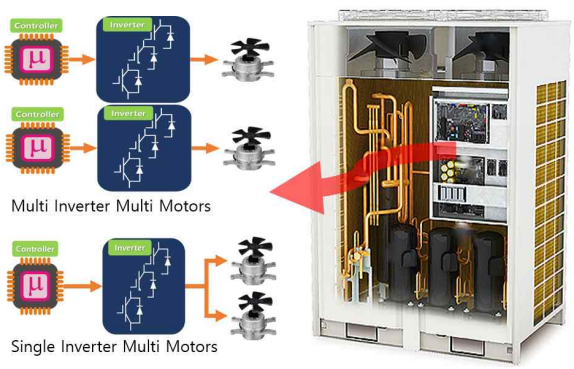

Fig. 1. Schematic of the SIMM system

† Corresponding Author: School of Electronics Engineering, Kyung-pook National University, Korea. (whkwon@ee.knu.ac.kr)
* Development Center, Control Technology, Control Technology Team 3, Doosan Machine Tools Korea. ({chul.yun, taesung.jang}@doosanmt.com)
** Dept. of Electronics Information, Keimyung College University, Korea. (nscho@kmcu.ac.kr)
*** School of Electronics Engineering, Kyung-pook National University, Korea. (gksjwl@nate.com)
Received: August 14, 2017; Accepted: March 13, 2018

proportional gain to ensure the stability of the system. Since a general controller generates a signal that is proportional to the error signal, the steady-state error is reduced by the proportional increase in the gain, but it forfend the large vibration. However, the conventional method has a drawback in that the gain is determined ambiguously and imprecisely; this occurs because the gain is extracted using an experimental empirical method in which the damping coefficient of the system is increased according to the proportional gain without accurate analysis of the resonance frequency characteristics of the SIMM system.

Therefore, in this paper, we propose a controller design method that suppresses the resonance that is caused by the auxiliary motor owing to the differences between loads and parameters during parallel operation of the SIMM system that is controlled by the master and slave method. The proposed resonance suppression controller gain is directly obtained by analyzing the resonance characteristics [8] using the phase controller realization method. The advantage of this approach is that the error associated with the gain determination can be fundamentally reduced. In addition, the proposed resonance suppression controller is robust with respect to variations in the system's parameters, because it is designed as a phase controller, and the stability region of the system becomes wider owing to the added zero point.

This paper is organized as follows. First, we design a phase controller that can increase the damping at the resonance point based on the results of the resonance analysis of the SIMM system, and we propose a method for setting the gain of the resonance suppression controller. Next, using Kharitonov's polynomials, we demonstrate the robustness of the proposed controller with respect to variations in the system's parameters [14]. Finally, we use simulations and experiments to validate the performance of the proposed controller and the system's robustness with respect to parametric variations.

2. Analysis of the system

2.1 Analysis of the SIMM system stability

As shown in Fig. 2, the coordinate axes d^r-q^r, rotating from the SIMM structure to the rotor angular velocity by the closed-loop control with the main motor, can be expressed using Eq. (1) [8].

$$\begin{bmatrix} v_d^r \\ v_q^r \end{bmatrix} = \begin{bmatrix} R_s + pL_s & -\omega_{re}^r L_s \\ \omega_{re}^r L_s & R_s + pL_s \end{bmatrix} \begin{bmatrix} i_d^r \\ i_q^r \end{bmatrix} + \omega_{re}^r \phi_f \begin{bmatrix} 0 \\ 1 \end{bmatrix} \quad (1)$$

where R_s is the stator resistance, L_s is the stator inductance, p is the differential operator, and ϕ_f is the permanent magnet flux linkage. The coordinate axes $d^\omega-q^\omega$, rotating

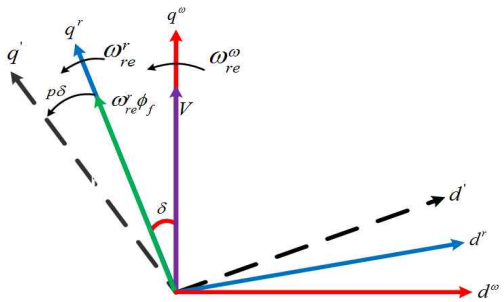

Fig. 2. Relation between d^r-q^r and $d^\omega-q^\omega$

at an arbitrary angular speed according to the open loop control from the SIMM structure to the slave motor, are given by Eq. (2).

$$\begin{bmatrix} v_d^\omega \\ v_q^\omega \end{bmatrix} = \begin{bmatrix} R_s + pL_s & -\omega_{re}^\omega L_s \\ \omega_{re}^\omega L_s & R_s + pL_s \end{bmatrix} \begin{bmatrix} i_d^\omega \\ i_q^\omega \end{bmatrix} + \omega_{re}^r \phi_f \begin{bmatrix} -\sin\delta \\ \cos\delta \end{bmatrix} \quad (2)$$

where ω_{re}^ω is the reference angular speed of the inverter.

From the error terms in Eqs. (1) and (2), the relationship between the torque and electric angular velocity for the two motors can be captured by Eqs. (3) and (4).

$$\begin{aligned} T &= T_e^r - T_e^\omega \\ &= \frac{3}{2} P_f \mathrm{f}_f i_q^r - \frac{3}{2} P_f \mathrm{f}_f \left(i_d^\omega \sin\delta + i_q^\omega \cos\delta \right) \end{aligned} \quad (3)$$

$$\begin{aligned} \frac{d\omega_{re}^r}{dt} &= \frac{P_f}{J} T \\ &= \frac{3}{2} \frac{P_f^2 \mathrm{f}_f}{J} \left\{ i_q^r - \left(i_d^\omega \sin\delta + i_q^\omega \cos\delta \right) \right\} \end{aligned} \quad (4)$$

where P_f is a pole pair. As shown in Fig. 2, in the open-loop control method, the q^ω axis coincides with the inverter output voltage's vector term, and the q^r axis coincides with the motor's back-EMF vector term in the closed-loop control method. Therefore, as shown in Fig. 2, a torque angle δ exists between the two axes d^r-q^r and $d^\omega-q^\omega$, depending on the difference between rotational speeds and the variation in the torque angle. This relationship can be expressed by Eq. (5).

$$p\delta = \omega_{re}^r - \omega_{re}^\omega \quad (5)$$

The transfer function can be expressed as Eq. (6) from the linear state equation for the relationship between electrical system and mechanical system of Eq. (1) ~ (6).

From the Eq. (6), the damping coefficient and the resonance frequency can be derived as Eq. (7).

$$G(s) = \frac{\Delta\omega_{re}^r}{\Delta\omega_{re}^\omega} = \frac{\frac{3}{2}\frac{P_f^2\phi_f^2}{JL_s}}{s^2 + \frac{3}{2}\frac{P_f^2\phi_f^2}{J}\frac{R_s}{\omega_0^2 L_s^2}s + \frac{3}{2}\frac{P_f^2\phi_f^2}{JL_s}} \quad (6)$$

Table 1. Nominal parameters of the SPMSM system

Parameter	Values
Rated power	900 [W]
Rated velocity	850 [rpm]
Phase resistance	1.425 [Ω]
Phase inductance	37 [mH]
Electro motive force constant	0.156 [V/rad]
Number of pole	8
Moment of inertia	0.03 [kg/m^2]

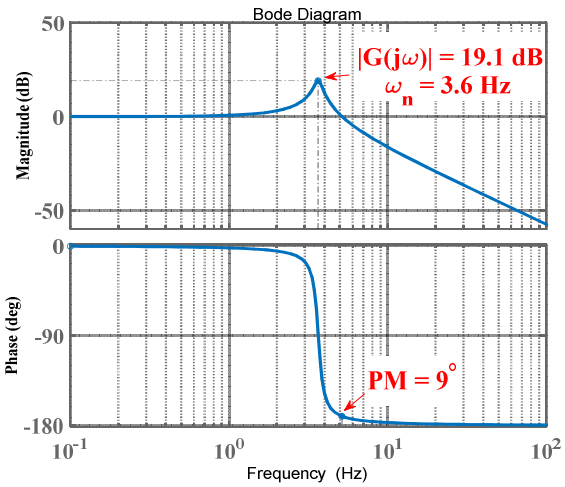

Fig. 3. Frequency response of the SIMM system

$$\zeta = \sqrt{\frac{3}{2}}\frac{\sqrt{JL_s}}{2}\frac{P_f\phi_f}{J}\frac{R_s}{\omega_0^2 L_s^2}$$
$$\omega_n = \sqrt{\frac{3}{2}}\frac{P_f\phi_f}{\sqrt{JL_s}} \quad (7)$$

The frequency response of the SIMM system is given by the Bode plot (Fig. 3), with Eq. (6) describing the transfer function and the system's parameters listed in table 1. The resonance frequency is 3.65 Hz, the magnitude is 19.1 dB, the phase margin is 9° and the damping coefficient is 0.0558. As a result, the SIMM system with master-slave control is unstable, because the damping coefficient is close to zero and because the phase margin is insufficient.

2.2 Proposed resonance suppression method

In general, the damping coefficient of the secondary system is approximately proportional to the phase margin. To increase the phase margin, a controller with zero added to the system, such as a PD controller, can be designed to ensure the stability of the system. However, such a PD controller is disadvantageous in that the noise increases because the gain increases at high frequencies.

Therefore, to resolve the problem of instability of the SIMM system and the amplification of noise at high frequencies, the lead controller was designed according to Eq. (8).

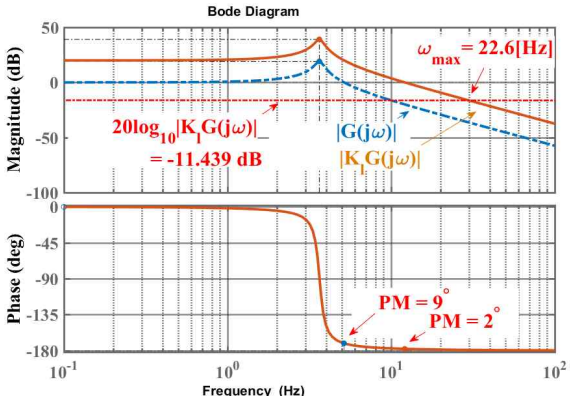

Fig. 4. Frequency response of the DC gain K

$$D(s) = K_l\frac{T_l s+1}{\alpha_l T_l s+1} \quad (8)$$

where K_l is the DC gain of the system.

The gain that yields the steady state error of 0.1 is $K_l = 10$, because the steady state error for the unit step input is $e_{ss} = \lim_{s\to 0} sE(s) = \frac{1}{1+K_l} \cong \frac{1}{K_l}$. The frequency response for the proportional gain is shown in Fig. 4. From the Bode plot of the open-loop function for the proportional gain K_l it follows that the system is unstable because the magnitude increases by 20 dB and the phase margin decreases by 7°, as shown in Fig. 4. Therefore, we set $\phi_{\max} = 60^\circ$ to increase the phase margin by 60°. Then, α_l (to limit the gain at higher frequencies) can be calculated from Eq. (9).

$$\alpha_l = \frac{1-\sin\phi_{\max}}{1+\sin\phi_{\max}} \quad (9)$$

The frequency that maximizes the phase margin of the lead controller by α_l can be derived from Eq. (10).

$$20\log_{10}\left|K_l G(j\omega)\right| = -\frac{1}{2}20\log_{10}\left(\frac{1}{\alpha_l}\right) \quad (10)$$

The frequency with the magnitude of Eq. (10) becomes the crossover frequency of the system with the maximal phase. It can be shown that α_l and $\omega_{\max}$ become a half of the crossover frequency. The frequency at which the phase is maximal is given by Eq. (11).

$$T_l = \frac{1}{\omega_{\max}\sqrt{\alpha_l}} \quad (11)$$

The lead controller parameters calculated from Eqs. (9)-(11) for the phase margin of 60° phase margin are listed in Table 2.

Table 2. Nominal parameters of the SPMSM system.

Parameter	Values
α_l	0.0718
$20\log_{10}\left\|K_lG(j\omega)\right\|$	-11.439 [dB]
$\omega_{\max}$	22.6 [Hz]
T_l	0.0263

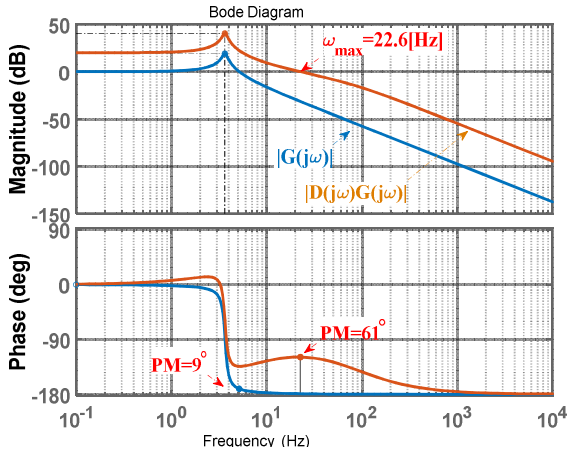

Fig. 5. Frequency response of the lead controller

The open-loop frequency response characteristics, described by Eqs. (6) and (8) for the SIMM system and the lead controller, are shown in Fig. 5. Comparing the $\left|G(j\omega)\right|$ response to the $\left|D(j\omega)G(j\omega)\right|$ response, the phase margin increased to 61° and the bandwidth of the system increased by a factor of ~6.2 when using the phase controller designed as described by Eqs. (9)-(11), and these differences are clearly captured in Fig. 5. As a result, the damping coefficient of the system increases as the phase margin of the lead controller increases, thereby improving the system's stability.

The second term in Eq. (3) is the torque equation of the auxiliary motor which is changed by the synchronous speed mismatch between the main motor and the auxiliary motor, as captured by Eq. (12) [11]. The first term in Eq. (12) is the magnetic torque component of the motor that generates the active power, and the second term is the torque that oscillates according to the phase difference between the two motors.

$$T_e^{\omega} \approx \frac{3}{2}P_f\mathrm{f}_f i_q^r + \frac{3}{2}P_f\mathrm{f}_f\left[\, i_d^r\delta - K\left(R_s\delta + \omega_{re}^r\mathrm{f}_f\right)\delta\,\right] \quad (12)$$

Using Eq. (12), the torque of the auxiliary motor can be expressed by the d^r-q^r axis current of the main motor. Thus, the main motor can be controlled using the q^r axis current of the main motor and the auxiliary motor can be controlled using the d^r axis current of the main motor. Therefore, the angle between the torques can be reduced, attenuating the difference between the speeds of the two motors, by controlling the auxiliary motor's torque.

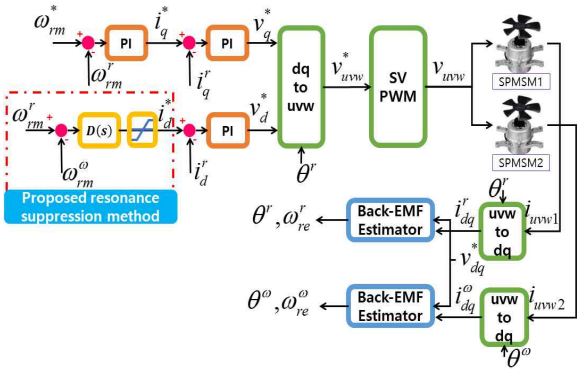

Fig. 6. Block diagram of the proposed control system

The control block diagram for the resonance suppression in the SIMM system is shown in Fig. 6, based on the analysis in Section 2.1 and based on the frequency response in the Bode plot for the lead controller.

In Fig. 6, ω_{rm}^r is the angular speed of rotation of the main motor and ω_{rm}^{ω} is the angular speed of rotation of the slave motor.

2.3 Robustness with respect to parametric variations

Using Kharitonov's polynomials [14], we confirmed the robustness of the proposed resonance suppression controller with respect to parametric variations. When the coefficient of the transfer function is being varied by system constant change, the Kharitonov's polynomial is obtained by the maximum value and the minimum value of the coefficient change range, and the extent of robustness was then determined using the obtained Kharitonov's polynomial. The n^{th} order interval polynomial is robustly stable if and only if its $Q_1(s)$ is stable for $n=3$ [15]. Eq. (13) describes the standard third-order system, and Eq. (14) shows the Hurwitz matrix, which serves as a criterion for determining whether Eq. (13) is satisfied.

$$Q_1(s) = a_0^M s^3 + a_1^m s^2 + a_2^m s + a_3^M \quad (13)$$

$$\Delta_2 = \begin{pmatrix} a_1^m & a_3^M \\ a_0^M & a_2^m \end{pmatrix} = a_1^m a_2^m - a_0^M a_3^M > 0 \quad (14)$$

In the above equations, M is the maximal value and m is the minimal value that are obtained upon changing the constant. Therefore, the system's robustness can be determined by calculating the coefficients of the equivalent resistance of the motor, the equivalent inductance, the flux of the permanent magnet, and the extent of variation in the inertia, as shown by Eq. (15).

$$\begin{aligned} a_0^M &= \alpha_l T_l \\ a_1^m &= 2\varsigma^m(\omega_n)^m\alpha_l T_l + 1 \\ a_2^m &= \alpha_l T_l(\omega_n^2)^m + 2\varsigma^m(\omega_n)^m + K_l T_l(\omega_n^2)^m \\ a_3^M &= (1+K_l)(\omega_n^2)^M \end{aligned} \quad (15)$$

Consequently, the proposed resonance suppression controller is robust because the coefficients of its transfer function satisfy Eqs. (13) and (14) even for ±50% variation of the system's parameters.

3. Experimental Validation

3.1 Simulation conditions

Two simulation studies were performed in this work. The first simulation aimed to confirm the validity and usefulness of the proposed resonance suppression controller gain. The second simulation aimed to assess the system's robustness with respect to parametric variations.

First, a simulation was performed to assess the usefulness of the proposed resonance suppression controller in a parallel operation system of a single inverter based permanent magnet synchronous motor. The speed and current controller were designed with a commonly used PI controller. The proposed resonance suppression controller was designed with a lead controller, as shown in Eq. (15). The SPMSM parameters used in this simulation are listed in Table 1. The main motor was defined as SPMSM1(M1) and the slave motor was defined as SPMSM2(M2). The two motors operated in parallel.

Next, simulations were conducted to validate the proposed resonance suppression controller gain design for ±50% variations in the motor parameters.

3.2 Simulation results

In Fig. 7, both motors were operated at 10% of the rated load up to 0.9 s, and after 0.9 s 11% of the rated load was applied only to M2 as a step signal.

After 0.9 s, the two motors exhibited a 2% difference between their loads, and operated in parallel at middle and low speed of 350 rpm. In other words, M2 exhibited resonance owing to the load difference between the two motors. Fig. 8(a) shows the angular velocity for both motors and Fig. 8(b) shows the angular velocity mismatch across the two motors.

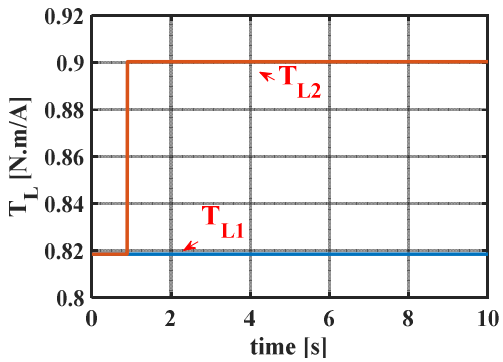

Fig. 7. Behavior of the load torque

After 0.9 s, the angular velocity mismatch oscillated at 3.4 Hz owing to the load difference. After 5 s, the

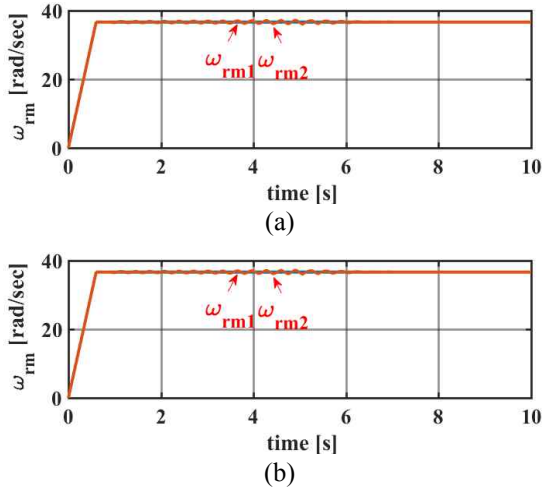

Fig. 8. Angular velocities. (a) Angular velocities for the two motors. (b) The error (mismatch) between the angular velocities of the two motors

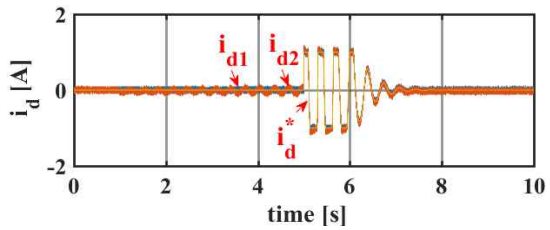

Fig. 9. D-axis currents, for the two motors

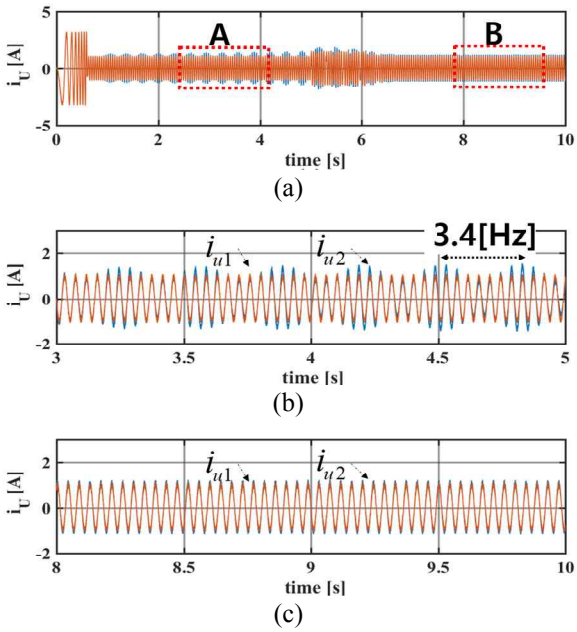

Fig. 10. U-phase currents. (a) The U-phase currents for the two motors. (b) A zoom-in view into region A. (c) A zoom-in view into region B

resonance was reduced by the resonance suppression controller; and after 7 s, the two motors stably operated in parallel without any mismatch between their angular velocities.

Fig. 9 shows the d-axis currents for the two motors. For M2, the d-axis current oscillated at 3.4 Hz, owing to the load difference between the two motors. The resonance was reduced by the resonance suppression controller starting from 5 s, and then the current eliminated the resonance at 7 s.

Fig. 10(a) shows the U-phase current of the two motors and Fig. 10(b) shows a zoom-in view into region A, while Fig. 10(c) shows a zoom-in view into region B. The U-phase current of M2 oscillated at a resonant frequency of 3.4 Hz. The oscillation decreased starting from 5 s, with the resonance suppression controller and the U-phase response exhibiting no resonance at 7 s.

The resonance occurred for $i_{ds}^{*} = 0$ under unbalanced load conditions between 0 seconds and 2 seconds, and the resonance suppression controller started to suppress the resonance at 2 seconds, as shown in Fig. 11.

Fig. 11 shows the mismatch between the angular velocities of the main and auxiliary motors when the equivalent resistance, the equivalent inductance, the flux of the permanent magnet, and the inertia coefficient were varied by ± 50% relative to their normal operational values.

From Figs. 11, it is clear that the resonance suppression controller eventually suppresses the mismatch between the angular velocities of the two motors to zero, even when the system's parameters are varied by ±50%. This confirms Kharitonov's robustness property.

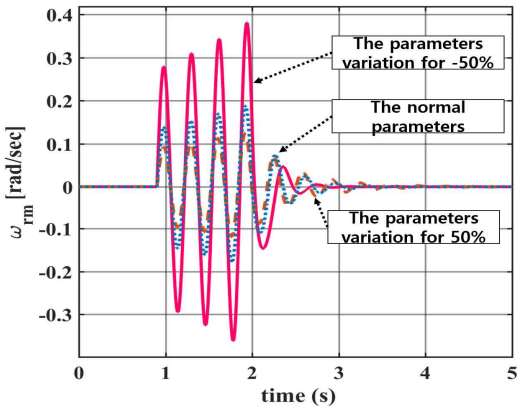

Fig. 11. Mismatch between the angular velocities of the two motors in the SIMM system vs. time, for ±50% variation in the system's parameters

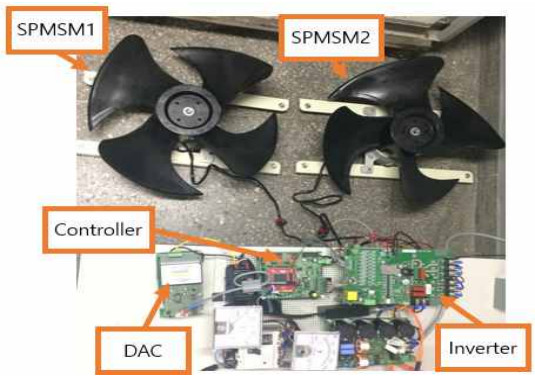

Fig. 12. Experimental system

3.3 Experimental conditions

The feasibility of the proposed system as a resonance suppression controller for parallel operation of two SPMSMs

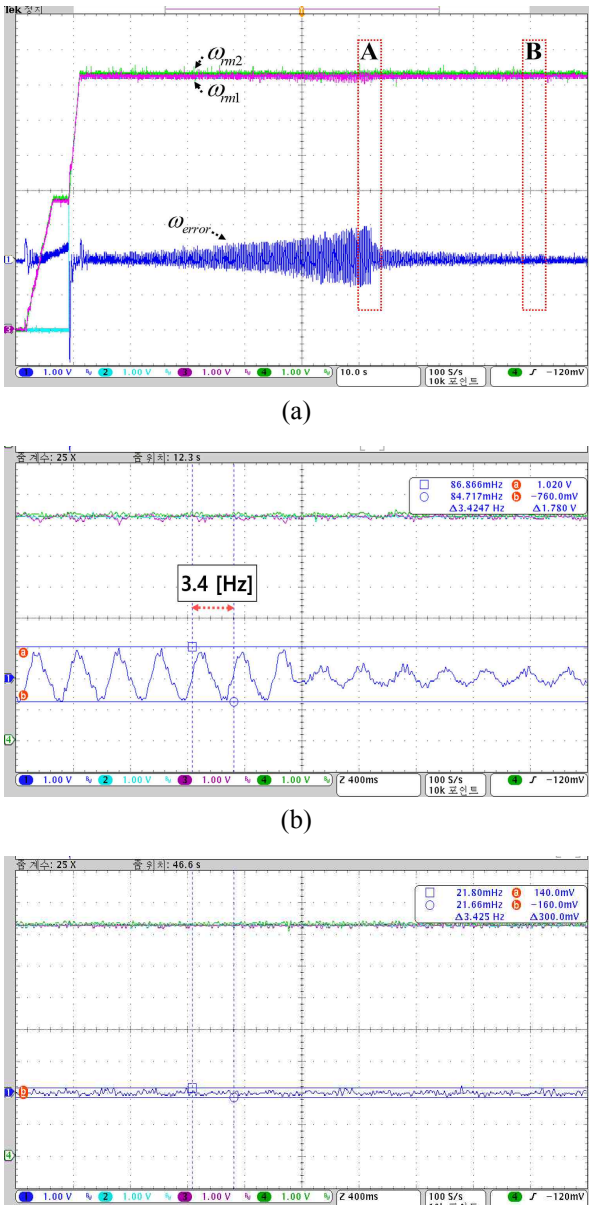

Fig. 13. Angular velocities. (a) Angular velocities and their mismatch, for the two motors. (b) A zoom-in view into region A. (c) A zoom-in view into region B

was validated experimentally.

The experimental system consisted of two 900-W-power SPMSMs, an inverter board, a control board, and a DAC board for data analysis, as shown in Fig. 12. The specifications of the motors used in this experiment were the same as those listed in Table 1. M2 was used as the main motor and M1 was used as the slave motor.

3.4 Experimental results

Fig. 13 shows the angular velocities of the two motors and their mismatch. Fig. 14 shows the d-axis currents of the two motors, and Fig. 15 shows the U-phase currents of the two motors.

On the initial start under sensorless control, a steady state was reached at 10 s, after the system accelerated to 350 rpm.

The mismatch between the angular velocities of the two motors oscillated for up to 60 s, with a resonance frequency of 3.4 Hz, as shown in Fig. 13(b). Fig. 13(c) shows that after 60 s, the vibration component was reduced by the resonance suppression controller, stabilizing the angular speeds of the two motors for parallel operation without mismatch.

Fig. 14(a) shows the d-axis currents of the two motors. In Fig. 14(b), the d-axis current of M1 oscillates at 3.4 Hz owing to the load difference and because the oscillation is reduced by the d-axis command current of the resonance suppression controller output from region A. Fig. 14(c)

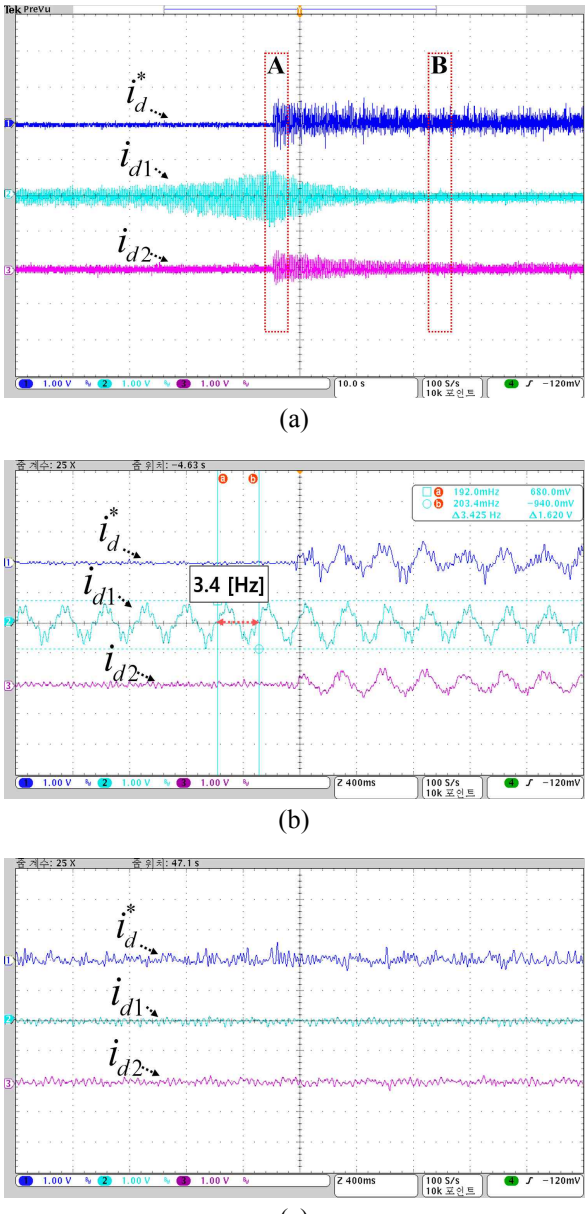

(a)

(b)

(c)

Fig. 14. D-axis currents. (a) D-axis currents and reference current, for the two motors. (b) A zoom-in view into region A. (c) A zoom-in view into region B

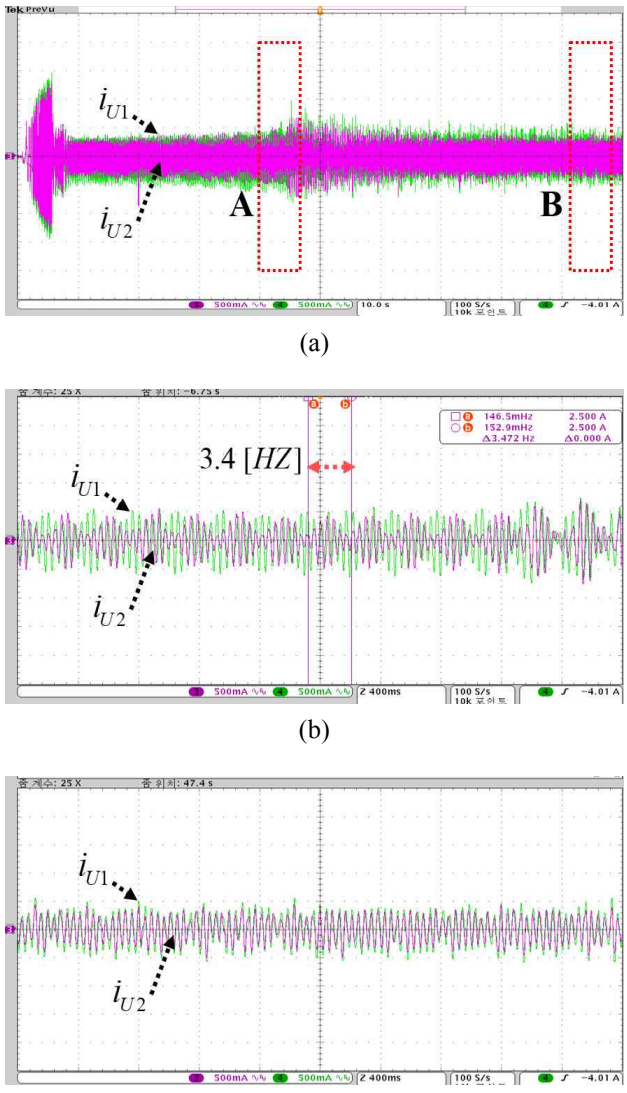

(a)

(b)

(c)

Fig. 15. U-phase currents. (a) U-phase currents for the two motors. (b) A zoom-in view into region A. (c) A zoom-in view into region B

shows the stable d-axis currents of the two motors. Fig. 15(a) shows the U-phase currents of the two motors. For M1, the U-phase current oscillates at 3.4 Hz owing to the load imbalance, and the vibration is decreased by the resonance suppression controller starting from region A, as shown in Fig. 15(b). The resulting stable U-phase current is shown in Fig. 15(c).

4. Conclusions

This paper addressed the design of a controller that suppresses the resonance phenomenon for middle and low speed parallel operation of two SPMSMs in the SIMM structure controlled using the master and slave method. When the auxiliary motor operates with a larger load than the main motor in the middle and low speed regimes in which the stator resistance cannot be ignored, the master and slave method induces resonance that engages the auxiliary motor, owing to a difference between the torque angles of the two motors. This resonance contributes to destabilizing the SIMM system.

To address this issue, in this paper we proposed a controller design method that suppresses the resonance generated by the auxiliary motor owing to different loads and parameters across the two motors during parallel operation in middle and low speed regime of two SPMSMs. The proposed resonance suppression controller gain was derived theoretically directly by analyzing the resonance characteristics, using the phase control method, which can significantly facilitate the design process. The proposed resonance suppression controller was determined to be robust with respect to variations in the system's parameters, because it was designed as a phase controller, and the stability region of the system increased owing to the added zero point. The system's robustness was confirmed using Kharitonov's polynomials and simulation. Finally, we validated the function and feasibility of the proposed resonance suppression controller by conducting simulations and experiments.

Acknowledgements

This work was supported in part by the Industrial Technology Innovation Program of Korea Evaluation Institute of Industrial Technology 10067754 (Ministry of Trade, Industry & Energy).

References

[1] Jones. M, Ishak. Vukosavic. S.N, Dujic. D, Levi. E, and Wright. P, "Five-leg inverter PWM technique for reduced switch count two-motor constant power applications," *IET Electr. Power Appl*., vol. 2, no. 5, pp. 257-287, Sep. 2008.

[2] Ahmad Asri Abd Samat, Dahaman Ishak, Pais Saedin, and Shahid Iqbal, "Speed-sensorless control of parallel-connected PMSM fed by a single inverter using MRAS," 2012 *IEEE International Power Engineering and Optimization Conference*, pp. 35-39, June 2012.

[3] Jurifa Matlagi, Zulkifilie Ibrahim, and Marizan Sulaiman, "Mean and differential torque control using hysteresis current controller for dual PMSM drives," *Journal of Theoretical and Applied information Technology.*, vol. 33, no. 1, pp. 76-82, Nov. 2011.

[4] Damien Bidart, Maria Pietrzak-David, Pascal Maussion, and Maurice Fadel, "Mono inverter dual parallel PMSM-Structure and Control strategy," *34th Annual Conference of IEEE. IECON 2008.*, pp. 268-273, Nov. 2008.

[5] D. Bidart, M. Pietrzak-David, P. Maussion, and M. Fadel, "Mono inverter multi-parallel permanent magnet synchronous motor: structure and control strategy," *IET, Electric Power Applications.*, vol. 5, no. 3, pp. 288-294, Mar. 2011.

[6] C. B. Kim, C. Yun, B. K. Yoon, N. S. Cho, and W. H. Kwon, "Parallel sensorless speed control using flux-axis current for dual SPMSMs fed by a single inverter," *Journal of Electrical Engineering & Technology*, vol. 10, no. 3, pp. 1048-1057, May 2015.

[7] Paresh C. Sen, "Principles of electric machines and power electronics Second Edition," John Wiley & Sons, pp. 479-493, 1998.

[8] C. Yun, and W.H. Kwon, "The Resonance Characteristic Analysis for Speed Control of Parallel Connected Dual SPMSMs fed by a single Inverter," *The Transactions of the Korean Institute of Electrical Engineers.*, vol. 66, no. 44, pp. 643-650, Apr. 2017.

[9] Y.J. Lee and J.I. Ha, "Analysis and Control of Mono Inverter Dual Parallel SPMSM Drive System," *Energy Conversion Congress and Exposition (ECCE), 2014 IEEE.*, pp. 4843-4849, Sep. 2014.

[10] Y.J. Lee and J.I. Ha, "Control Method for Mono Inverter Dual Parallel Surface-Mounted Permanent Magnet Synchronous Machine Drive System," *IEEE Transactions on Industrial Electronics.*, vol. 62, Issue 10, pp. 6096- 6107, Apr. 2015.

[11] C. Yun, W.H. Kwon, and N.S. Cho, "The Vibration Suppression using Reactive Power Compensator for Speed Control of Parallel Connected Dual Fan Motors fed by a Single Inverter," *The Transactions of the Korean Institute of Electrical Engineers.*, vol. 65, no. 12, pp. 2008-2013, Dec. 2016.

[12] T. Nagano, and J.I. Itoh, "Parallel connected multiple drive system using small auxiliary inverter for number of PMSM," *Power Electronics Conference* (*ECC-ASIA*), *2014 IEEE.*, pp. 1253-1260, May 2014.

[13] T. Nagano, G.T. Chiang, and J.I. Itoh, "Parallel

connected multiple drive system using small auxiliary inverter for permanent magnet synchronous motor," *Journal of Industry Applications.*, vol. 4, no. 1, pp. 40-48, Jun. 2015.
[14] R.Temppo and F Blanchini, "Interval Polynomials : Kharitonov's Theorem and Value Set Geometry," *The Control Handbook. CRC Press. Bocal R Atino. FL.*, pp. 501-502, 1996.
[15] Dmitri P. Kim, "Automatic Control Theory of Linear Control System," HANOL, pp. 253-261, 1998.

Chul Yun He received Ph.D. degree in electrical engineering with School of Electronics Engineering (SEE), Kyungpook National University (KNU), Daegu, Korea, in 2018, and currently work for Doosan Machine Tools. His research interests are servo motor control, power electronics.

Tae-Sung Jang He received M.S. degree in Electrical Engineering, Myongji University, Seoul, Korea, in 1996, and currently work for Doosan Machine Tools. His research interests are computer numerical control, servo motor control.

Nae-Soo Cho He received B.S degree in electrical engineering from Kyungil University. Kyungpook, Korea, in 2001, and the M.S. and Ph.D. degree in electrical engineering with School of Electronics Engineering (SEE), Kyungpook National University (KNU). Daegu, Korea, in 2003 and 2012, respectively. He has been with the Dept. of Electronics Information in the Keimyung College University since 2013, where he is now a Professor. His research interests are motor control and embedded systems.

Byun g-Keun Yoon He received B.S degree in electrical engineering from Daegu University, Kyungpook, Korea, in 2010, and M.S. degree in electrical engineering with School of Electronics Engineering (SEE), Kyungpook National University (KNU), Daegu, Korea, in 2013, and currently a Ph.D course student in the same university. His research interests are motor control, power electronics.

Woo-Hyen Kwon He received B.S degree in electrical engineering from Sogang University. Seoul, Korea, in 1978, and the M.S. and Ph.D. degree in electrical engineering from the Korea Advanced Institute of Science and Technology(KAIST). Seoul, Korea, in 1979 and 1993, respectively. He has been with the School of Electronics Engineering (SEE), in the Kyungpook National University(KNU), since 1979, where he is now a Professor. His research interests are in the area of static power converters and drives, and computer applied systems.